Cement and Concrete Research 157 (2022) 106827

Contents lists available at ScienceDirect

Cement and Concrete Research

journal homepage: www.elsevier.com/locate/cemconres

Effect of temperature on CO_2 curing, compressive strength and microstructure of cement paste

Bao Lu [a,b], Sarra Drissi [a,c,d,*], Jianhui Liu [a,c], Xiang Hu [a,c], Baixin Song [f], Caijun Shi [a,c,e,**]

[a] Key Laboratory for Green & Advanced Civil Engineering Materials and Application Technology of Hunan Province, Changsha 410082, China
[b] Key Laboratory for Advanced Technology in Environmental Protection of Jiangsu Province, Yancheng Institute of Technology, Yancheng 224051, Jiangsu, China
[c] College of Civil Engineering, Hunan University, Changsha 410082, China
[d] Department of Civil Engineering and Energy Technology, Faculty of Technology, Art and Design, Oslo Metropolitan University, PO box 4 St. Olavs plass, Oslo, NO-0130, Norway
[e] Department of Civil Engineering, The University of British Columbia, 6250 Applied Science Lane, Vancouver, BC V6T 1Z4, Canada
[f] School of Materials Science and Engineering, Henan Polytechnic University, Jiaozuo 454003, China

ARTICLE INFO

Keywords:
CO_2 curing
Temperature
Calcium carbonate crystals
Silica gel
Microstructure

ABSTRACT

This study investigated the effect of temperature (5 °C–50 °C) on the carbonation process, compressive strength and microstructure of CO_2-cured cement paste. Results showed that the carbonation process and rate were significantly affected by temperature and time. When the curing temperature increased, the rate of improvement of cement paste's properties was accelerated. The carbonation reaction was mainly kinetically controlled by product layer diffusion with an activation energy of about 10.8 kJ/mol. Temperature had greatly affected the structural transformation, morphological changes, size and amounts of calcium carbonate polymorphs (calcite, aragonite and vaterite) as well as their degree of crystallinity and decomposition temperature. Alongside calcite, vaterite and aragonite were formed at low and high curing temperatures, respectively. Apart from microstructure, the compressive strength was also found to be very sensitive to temperature and carbonation products. The relationship between the amount of different carbonate polymorphs and the compressive strength was also provided.

1. Introduction

CO_2 curing of concrete enables fast chemical reactions between the calcium-bearing phases in fresh concrete and CO_2 which accelerates its strength development and hence shortens the curing process [1,2]. This curing technique is receiving increased attention from researchers and practitioners as it can be a promising technology to reduce atmospheric CO_2 and improve the concrete properties significantly compared to conventional curing technologies, particularly steam curing [3,4].

Generally, CO_2 curing efficiency is strongly affected by numerous factors such as CO_2 concentration and pressure, mix design, moisture content, chemical composition, etc. [2,5–7]. Shi et al. [8] reported that the increase in the CO_2 pressure from 0.2 MPa to 0.5 MPa at the early ages of curing, particularly the first 30 min, improved the CO_2 uptake of lightweight concrete blocks. However, Salman et al. [9] found that using high CO_2 pressure caused capillary condensation in steel slag samples, which blocked the capillary pores and hindered the CO_2 diffusion. Besides, they noticed the presence of densely packed bud-shaped calcite crystals on the surface while less abundant and smaller irregular calcite crystals formed in the core of the sample [9]. This created strong and weak zones in the samples and consequently lowered the compressive strength [9]. Another study by Shao et al. [10] showed that the use of type 30 cement increased the CO_2 uptake and compressive strength by approximately 10% compared to type 10 cement. Furthermore, Shi et al. [11] observed a significant improvement in the degree of carbonation and compressive strength of concrete following a preliminary drying step prior to the curing process. This was due to the removal of capillary water from a large number of pores which decreased the moisture content and promoted the CO_2 diffusion into the cement matrix [11].

Temperature may also have strong effects on CO_2 curing [12].

* Correspondence to: S. Drissi, Key Laboratory for Green & Advanced Civil Engineering Materials and Application Technology of Hunan Province, Changsha 410082, China.
** Correspondence to: C. Shi, Department of Civil Engineering, The University of British Columbia, 6250 Applied Science Lane, Vancouver, BC V6T 1Z4, Canada.
E-mail addresses: sarahdrissi@hotmail.fr (S. Drissi), cshi@hnu.edu.cn (C. Shi).

https://doi.org/10.1016/j.cemconres.2022.106827
Received 19 September 2020; Received in revised form 3 April 2022; Accepted 26 April 2022
Available online 5 May 2022

Studies showed that the temperature affected significantly the diffusivity of CO_2 and the solubility of calcium ions in concrete. In fact, high temperature could reduce the solubility of CO_2 and calcium ions but could promote, on the other hand, the CO_2 diffusivity through the carbonated layers [13,14]. Liu et al. [15] reported that the CO_2 uptake increased from 2% to 14% as the curing temperature increased from 20 °C to 60 °C, but decreased from 14% to 6% as the temperature increased from 60 °C to 100 °C. This was attributed to the lower solubility of CO_2 in water at elevated temperatures. Salman et al. [9] found that increasing the curing temperature from 20 °C to 40 °C did not result in any noticeable increase in CO_2 uptake, but increased linearly with the temperature increase up to 80 °C. Humbert et al. [16] demonstrated that curing temperature above 60 °C hindered the carbonation reaction because of the fast evaporation of water.

According to the literature [17,18], temperature could control also the calcium carbonate ($CaCO_3$) dissolution and precipitation reactions. Generally, three crystallin polymorphs could be formed: calcite, vaterite and aragonite. Other allotropic varieties in hydrated forms were also reported by some researchers, namely amorphous calcium carbonate, calcium carbonate monohydrate and calcium carbonate hexahydrate [17,18]. Several favorable conditions for the production of synthetic $CaCO_3$ polymorphs have been proposed in the literature. Calcite was found to be the most thermodynamically stable crystalline phase under ambient temperature and standard pressure conditions. The best conditions promoting the formation of vaterite were temperatures up to 40 °C and pH between 8 and 10 [17]. Nevertheless, vaterite could be easily converted to calcite or aragonite in the presence of water [17]. On the other hand, 80 °C favored the formation of aragonite [19]. Compared to synthetic $CaCO_3$, these conditions could probably shift for cementitious materials owing to their complexity and the physical/chemical interactions between CO_2, cement particles and curing parameters. Furthermore, the effect of temperature on the carbonation process and compressive strength as well as the factors controlling these characteristics are still not clear. Therefore, the effect of temperature on the morphological changes of calcium carbonate polymorphs and kinetics of the carbonation process is investigated in this study. The sensitivity of CO_2 curing process to temperature was examined using the activation energy which is calculated using the Arrhenius equation. On the other hand, a correlation between the compressive strength and carbonates in carbonated calcium silicate binders was established in a previous study by Ashraf and Olek [20]. However, only the ratio of poorly and well crystalline carbonates was quantified. Therefore, this study aims to analyze quantitatively the relationship between compressive strength development and different calcium carbonate polymorphs.

2. Materials and specimen preparation

2.1. Materials

Portland cement (P·I 42.5) in accordance with GB 175–2007 having a specific surface area of about 336 m^2/kg was used in this study. Its chemical, main mineral composition and particle size distribution are summarized in Table1 and Fig. 1, respectively.

2.2. Specimen preparation

The cement pastes were prepared using a water to cement ratio of 0.18, which has been proven to be beneficial for CO_2 curing. All pastes were hand-mixed for 5 min at a room temperature of 20 ± 2 °C with a relative humidity of 70 ± 5%. Then, the dry mixture was filled into 20 mm diameter and 30 mm height cylindrical steel molds. Subsequently, the molds were uniformly compacted using a pressure machine at a pressure of approximately 10 MPa. Compaction was selected in this study to simulate the production of concrete blocks and ensure faster sample demolding [11,21,22]. The samples were then demolded and pre-conditioned for 2 h as specified in previous studies [11,23].

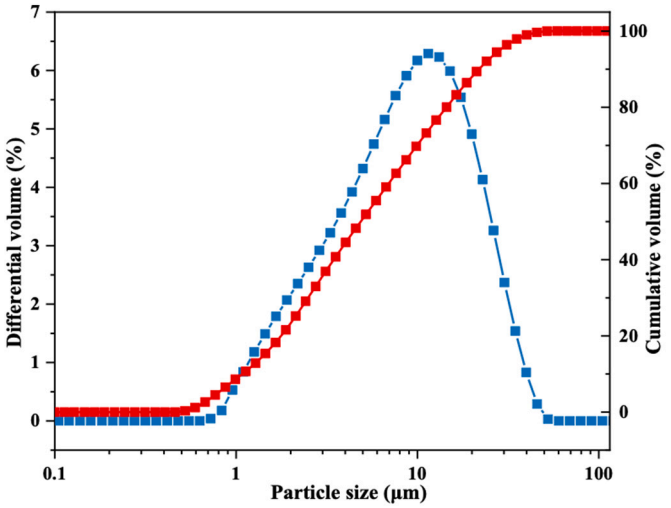

Fig. 1. Particle size distribution of Portland cement.

2.3. Curing process

The samples for most tests were placed in a CO_2 chamber with all surface exposed, in which the relative humidity, CO_2 concentration and pressure were maintained at 60% ± 5%, 20 ± 2% and 0.15 MPa, respectively. A thermostat was used to control the temperature of the CO_2 chamber at 5 °C, 20 °C and 50 °C. Samples were taken out for testing at 1 h, 2 h, 12 h, 24 h, 168 h and 672 h in order to investigate the evolution of their properties with time. Fig. 2 shows the temperature change of the sample center during the carbonation curing. The temperature increased quickly during the first few minutes then dropped to the set temperature in about 1 h and remained constant thereafter. Note that specimens for the carbonation depth measurements had only one end exposed to CO_2 but all other surfaces were sealed with paraffin.

3. Methods

The different tests conducted in this study are summarized in Fig. 3 and will be detailed in the following sections.

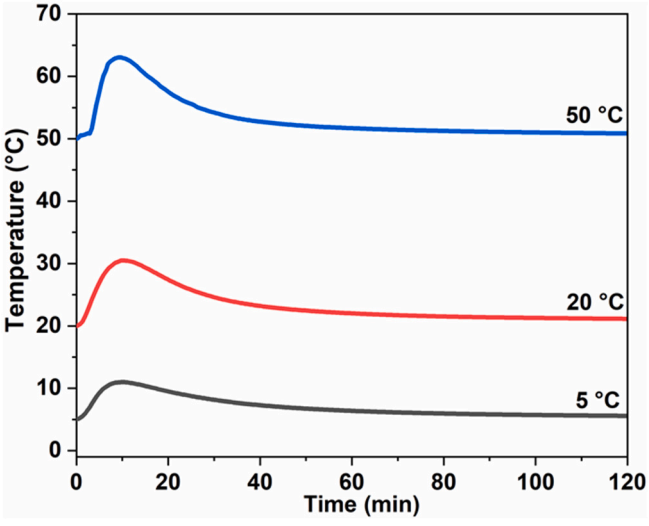

Fig. 2. Temperature change of samples during carbonation curing.

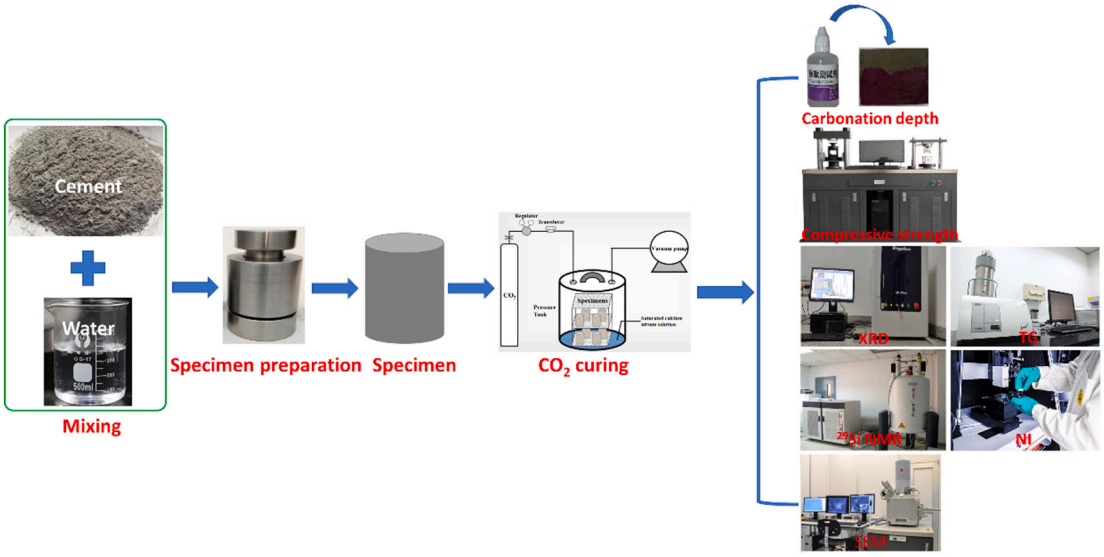

Fig. 3. A sketch of the experimental procedure.

3.1. Carbonation depth

At the end of each curing period, the sealed samples were taken out from the CO_2 chamber and cooled to room temperature. After splitting the samples, the split surfaces were cleaned and then sprayed with phenolphthalein solution (1% in 70% ethyl alcohol) [24]. The average depth of the colorless region was measured immediately after spraying phenolphthalein solution.

3.2. Compressive strength

The compressive strength of the samples was determined after 1 h, 2 h, 12 h, 24 h, 168 h and 672 h of full exposure to CO_2 for curing using a compression machine at a loading rate of 0.6 KN/s until failure. Three cylindrical samples were tested for each curing temperature and the mean value was reported as the compressive strength result.

3.3. Phase analysis and morphology characteristics

Thin layers were cut from the surface of the sample after fully exposure to CO_2 using an STX-202A small diamond wire cutting machine. The thickness of the layers was about 0.5 mm for X-ray diffraction (XRD), Thermogravimetric analysis (TGA) and Nuclear magnetic resonance (NMR) analyses and 2 mm for Scanning electron microscopy (SEM) analyses. The layers were then immersed in acetone and their weight change over time was tracked. The sample weight reached equilibrium after 7 d. During exchange, the solvent was renewed every 2 d. Afterward, the samples were dried in an oven at 60 °C for 72 h to remove acetone. For XRD, TGA and NMR analyses, the samples were grounded by pestle and mortar into a fine powder with a particle size of less than 45 μm.

3.3.1. XRD

XRD measurements were carried out on powdered samples using a Cu kα X-ray radiation at 40 Kv and 40 mA. The 2θ scans were carried out between 5°–65° with a step size of 0.02° at a rate of 2°/min. Rietveld analyses were carried out to provide semi-quantitative analysis of the crystalline phases by using rutile (20% by mass of the powder) as reference.

3.3.2. TGA

TGA was performed using approximately 15 mg of the powdered sample at a heating rate of 10 °C /min from 30 °C to 1000 °C under a 20 ml/min flow of nitrogen gas.

3.3.3. ^{29}Si NMR

Solid-state ^{29}Si magic angle spinning (MAS) NMR spectra were recorded on powdered samples at 79.5MHZ on a Bruker AVANCE III 400 MHz spectrometer with a B0 field strength of 9.4 T and MAS frequency of 8 kHZ in 3.2 mm rotors. The measurements were conducted using a 71.4 kHZ spinning rate, 1200 scans, $\pi/2$ pulses of 4.0 μs and 30s relaxation delays. The deconvolution method was used to calculate the proportion of Q^n in the different samples [25].

3.3.4. SEM-EDS

The morphology and chemical compositions of the samples were detected using a FEI Nova Nano SEM 450 equipped with a Backscattered electron detector (BSE) and an energy dispersed spectroscopy (EDS). Before testing, the samples were first embedded under vacuum in epoxy resin, then polished with 200, 400, 800, 1200 and 2000 grit sandpaper, and a Buehler EcoMet 30 polisher and finally coated with a thin layer of carbon. For each sample, more than 100 points were collected for the EDS analysis and were selected around the uncarbonated cement grains.

3.3.5. Nanoindentation

Nanoindentation tests were performed using a Switzerland CSM OPX/CPX system fitted with a Berkovich diamond indenter probe to evaluate the micromechanical properties of the sample. The tip was calibrated using a standard fused quartz specimen with known mechanical properties. Before testing, the sample was treated to achieve a roughness lower than 70 nm and ensure that its surface is adequately flat. Indentation grids of (10×10) indent spaced by 0.1 × 0.1 mm^2 were performed to characterize the different phases in each sample (Fig. 4). For each grid, a maximum force of 500 mN (maximum penetration depth of 1 μm) was held for 300 nm with the Berkovich tip. The loading and unloading were performed at a constant rate of 20 mN/s. The mean elastic modulus values of the sample and the individual microscopic phases were determined as described by Ashraf and Olek [20].

4. Results

4.1. Carbonation depth

Figs. 5 presents the carbonation depth images of cement paste samples cured at different temperatures. Besides, the carbonation depth versus the square root of curing time is shown in Fig. 6. As can be seen,

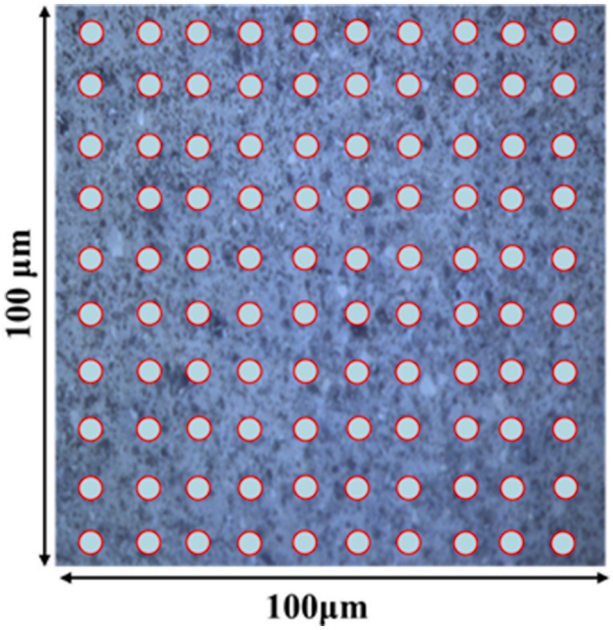

Fig. 4. Optical image of a region in indentation grids.

the samples were not completely carbonated at the depth. The carbonation depth was below 22 mm which is substantially lower than the height of the samples even after 28d of CO_2 curing. The reason for such result will be explained in detail in the following sections. On the other hand, Fig. 6 shows that the carbonation reaction was very fast during the first hour of curing. Nevertheless, this rate seems to slow down at a longer curing time which could be attributed to the precipitation of carbonation products which blocked the fast and further reaction of CO_2 with the matrix over time.

Fig. 7 shows that the carbonation depth increased with temperature regardless of age. For example, the carbonation depth of the sample after 28 days of CO_2 curing at 5 °C, 20 °C and 50 °C was 12.2 mm, 18.5 mm and 21.8 mm, respectively. Furthermore, samples cured at 50 °C reached a carbonation depth approximately up to 2 times as those cured at 5 °C, suggesting that higher curing temperature resulted in a faster carbonation rate.

4.2. Compressive strength

Fig. 8 shows the effect of curing temperature on the compressive strength of carbonated pastes. It is apparent that CO_2 curing contributed to a significant strength gain at early ages up to 24 h. The compressive strengths of paste carbonated for 2 h at 5 °C and 20 °C were nearly four and three times as those after 2 h of moist-curing, as shown in Figs. 8 and 9. Note that the samples used for the compressive strength measurement were fully exposed to CO_2 without any coating during the carbonation curing. The phenolphthalein changes the colour at lower pH values of approximately 9.0. While the colorless portion observed in the carbonated area of the Portland cement concrete corresponded to the pH range of 7.0–8.0 [26]. The non-carbonated part of the cement paste exhibited an alkalinity of pH > 11.5 and a magenta coloration was obtained [27]. Therefore, the actual carbonated depths are larger than the measured

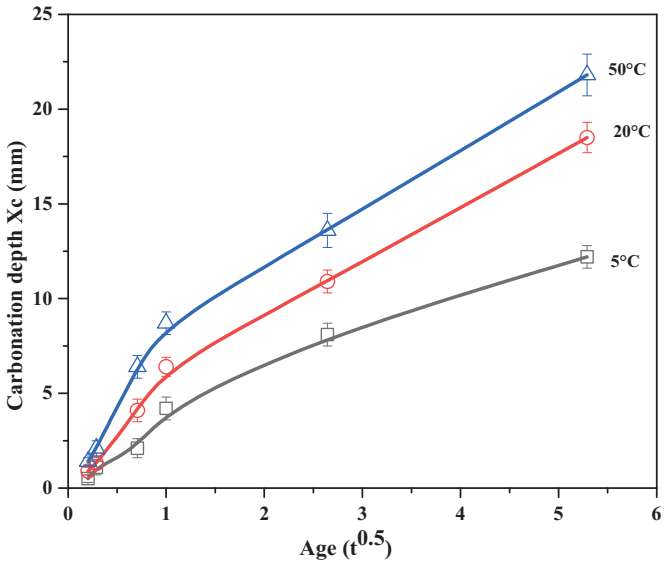

Fig. 6. Effect of temperature on carbonation depth.

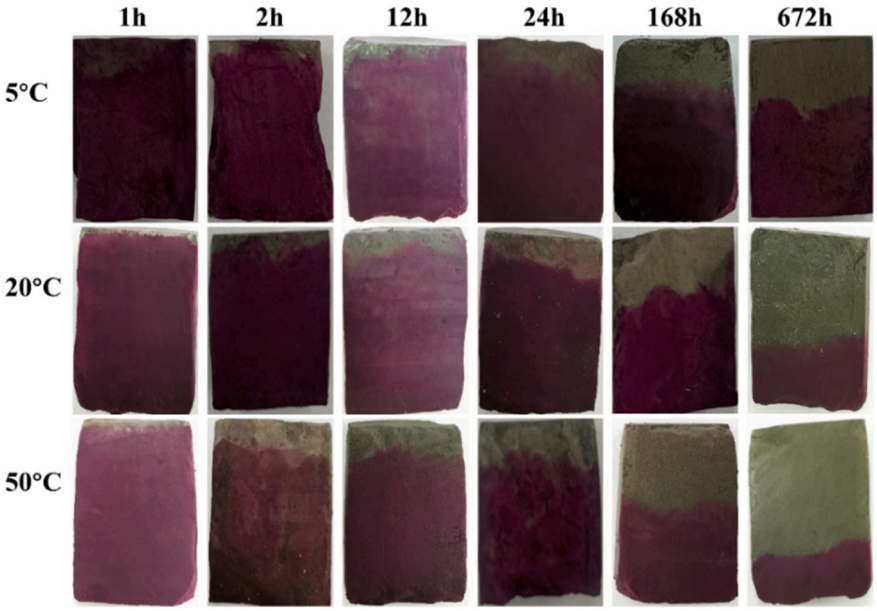

Fig. 5. Carbonation depths of cement samples cured at different temperatures.

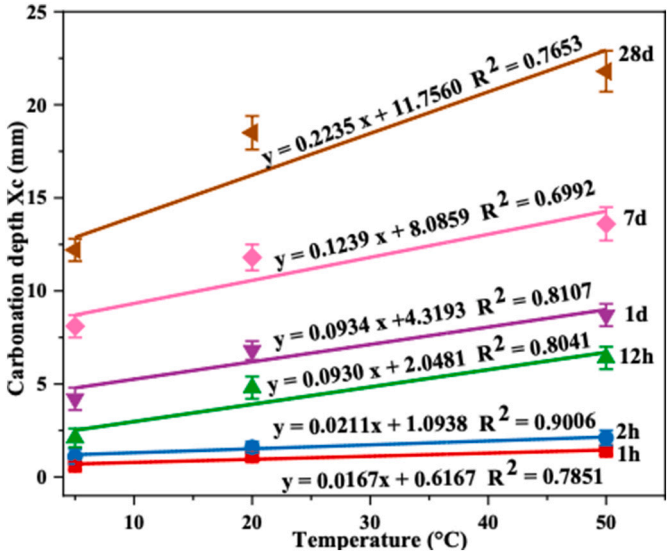

Fig. 7. Carbonation depth versus temperature.

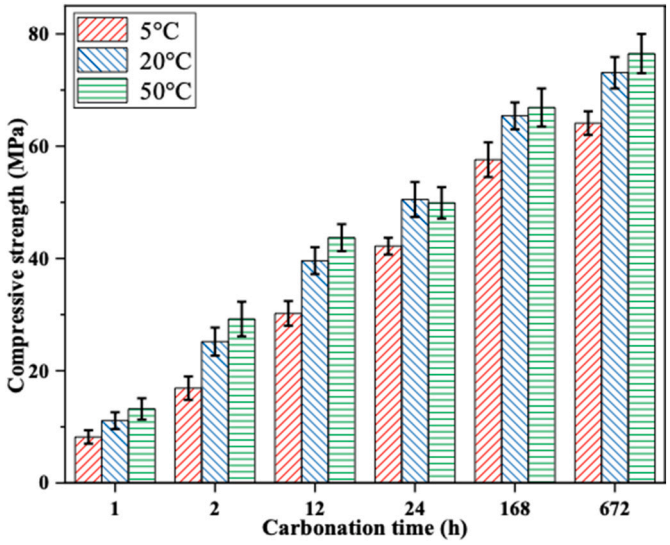

Fig. 8. Effect of temperature on compressive strength development of the CO_2-cured specimens.

ones. On one hand, the high strength of CO_2-cured specimens after a short period of time is attributed to the strong carbonated surface layer formed during carbonation. On the other hand, carbonation of cement is a very fast and exothermic process. Accelerated hydration of the cement in the uncarbonated portion due to its rapid temperature raise, as illustrated in Fig. 2, can also contribute to the early strength gain. Monkman and Shao [28] prepared concrete mixed with water to cement (w/c) ratio of 0.125 and found that the compressive strength of 2 h CO_2-cured sample was approximately 90.7% of the 24 h CO_2-cured sample. Zhan et al. [29] used CO_2 curing on the fresh OPC pastes prepared with a w/c ratio of 0.18 and found that their compressive strength after 2 h of carbonation curing achieved more than 66.1% of that after 24 h of carbonation curing. Pan et al. [6] found that the compressive strength of 3 h CO_2-cured sample was 18% higher than that of moist-cured samples though the carbonation depth was about 1.6 mm. With time, the compressive strength of moist-cured and CO_2-cured samples became almost similar due to the continued higher hydration rate of cement in moist-cured samples, but slowed down carbonation rate because of hindrance effect of the outer carbonated layer.

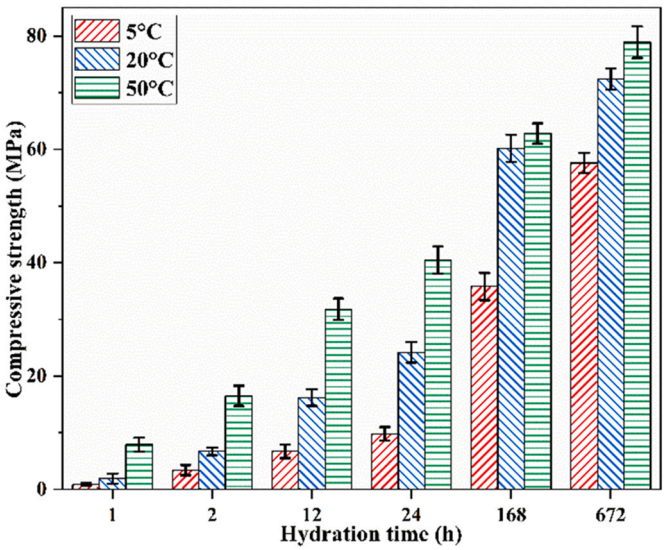

Fig. 9. Effect of temperature on compressive strength development of the moist-cured specimens.

On the other hand, it is clear that the low temperature affected negatively the compressive strength at both early and later-ages compared to high temperature. The early strength of the paste cured for 1 h at 20 °C and 50 °C was 35.4% and 60.9% higher than that cured at 5 °C, while their strength at 672 h was 14.1% and 16.2% higher than that cured at 5 °C. This might be possibly due to the acceleration of reaction rate at higher curing temperature which probably could result in major morphological changes in $CaCO_3$ crystals as well as their content in the samples. On the other hand, the temperature affected significantly the rate of strength development over time. As observed in Fig. 8, a rapid strength gain occurred at early ages, especially during the first 12 h of curing. Interestingly, at 20 °C and 50 °C a strength greater than 20 MPa was achieved after only 2 h of CO_2 curing, indicating that CO_2 curing could significantly reduce the curing time as reported by Shi et al. [8]. Afterward, this gain rate gradually decreased for all curing temperatures with curing time. In fact, the 12 h strength was almost 3.3 times the 1 h strength but the 24 h strength was only 1.4 times the 12 h strength. This could be attributed to the formation of $CaCO_3$ and the densification of the microstructure at early ages which probably hindered the further ingress of CO_2 in the sample and formation of carbonation products.

4.3. Phase evolution analyses by XRD and TGA

XRD patterns and quantitative XRD results are plotted in Figs. 11 and 12. Again, the experimental data reveal that samples were not fully carbonated since C_3S and C_2S were detected in the XRD patterns. As can be seen, the main phases present in all CO_2-cured samples were C_3S and C_2S as well as $CaCO_3$. Compared to cement mineral composition in Table 1, C_2S appeared to be much more reactive than C_3S towards carbonation which is consistent with the results reported previously [23]. Within the initial 2 h of curing, the total amount of $CaCO_3$ was about 9.8%, 17.9% and 23.4% in the sample cured at 5 °C, 20 °C and 50 °C, respectively, revealing that $CaCO_3$ formed immediately following CO_2 curing. In addition, a substantial increase in $CaCO_3$ peaks and a decrease in the C_3S and C_2S peaks over time were observed. A slightly lower amount of C_3S and C_2S, but a higher amount of $CaCO_3$ were detected in the sample cured at 20 °C and 50 °C compared to that cured at 5 °C, revealing that higher curing temperature significantly accelerated the conversion of clinker phases to $CaCO_3$. Moreover, it is clear that the three $CaCO_3$ polymorphs (vaterite, calcite and aragonite) were formed with calcite being the predominant carbonate in all pastes as

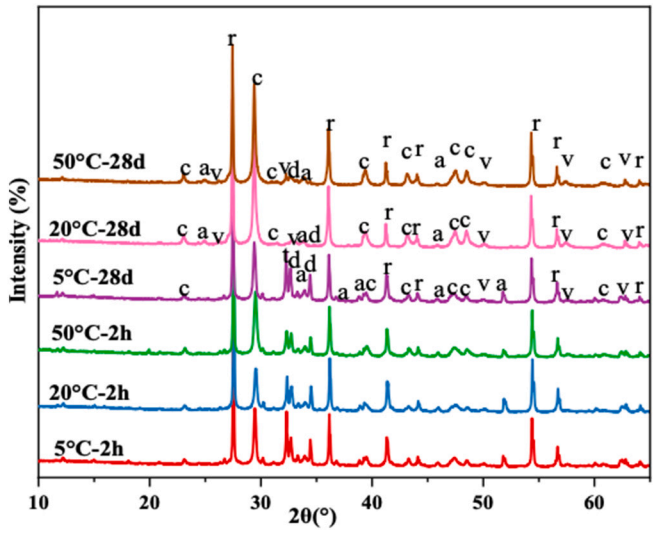

Fig. 11. XRD patterns of pastes CO_2-cured at different temperatures (a = aragonite; c = calcite; v = vaterite; t = C_3S; d = C_2S; r = Rutile).

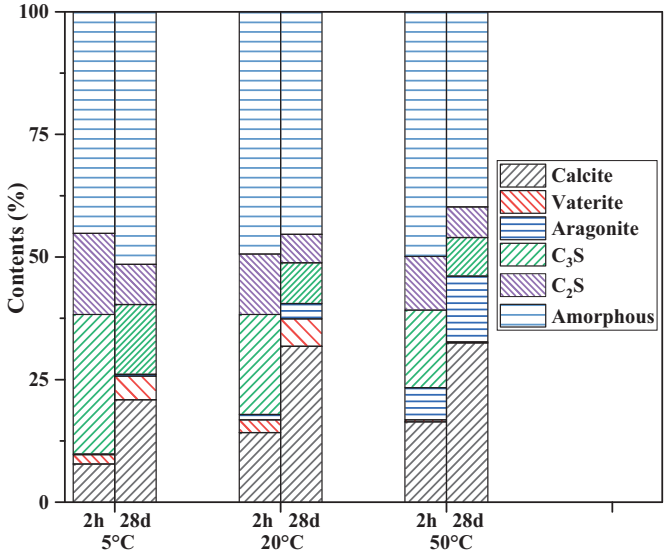

Fig. 12. Qualitative XRD results of pastes CO_2-cured at different temperatures.

reported in [29,30].

Figs. 11 and 12 show that temperature influenced strongly the crystallization pathway. This result matches well with other published studies [31,32] and SEM results (presented in section 4.5). An increase in temperature from 5 °C to 50 °C tended to favor the formation of aragonite rather than vaterite. According to [31,33], vaterite was the primary carbonation product that would transform to calcite at low temperatures and aragonite at high temperatures. At temperature between these limits, the three polymorphs (calcite, vaterite and aragonite) coexisted.

Fig. 13 depicts the TG-DTG results of cement pastes cured under different temperatures. After 2 h of curing, a certain mass loss around 88 °C - 106 °C was observed and could be resulted from the loss of free water or bound water from C-S-H. Note that this mass loss became negligible at 28d for samples cured at 5 °C and 20 °C suggesting a probable consumption of early hydration products (C-S-H phases) during CO_2 curing. However, a wider peak around 103 °C was observed for samples cured at 50 °C. The exact cause of this mass loss is not clear but could be mainly associated with the free water in the mix and possibly also from the formation of C-S-H. Besides carbonates, researchers observed the presence of silica gel as one of the main amorphous phases following the CO_2 curing of clinker phases and OPC paste [34]. According to Goto et al. [30], C-S-H gel was formed in the initial (3 min) stage of carbonation and then converted to silica gel [30]. The experimental results presented in [35,36] revealed the existence of amorphous calcium silicate hydrocarbonate and C-S-H gel in carbonated C_3S and C_2S. Therefore, it can be speculated that hydration could be probably undergoing simultaneously with carbonation at high temperatures. NMR results will provide further confirmation for this observation. Furthermore, no traces of $Ca(OH)_2$ could be specifically identified at all studied temperatures neither in the TGA results nor in the XRD patterns. No mass loss was detected between 200 °C and 450 °C. This could be a possible evidence of the fast carbonation reaction kinetics and the formation of carbonates prior to the formation of $Ca(OH)_2$ in the CO_2-cured samples. An important mass loss between 500 °C and 950 °C, corresponding to the decomposition of $CaCO_3$ [37–39], was observed. Most importantly, a slight shift in the decomposition temperature of $CaCO_3$ was also observed. For example, the $CaCO_3$ decomposition temperature of 28d CO_2-sample cured at 50 °C was around 740 °C which is 3% higher than that cured at 5 °C (Fig. 13 (b)). This suggests that high temperatures could improve to some extent the crystallization degree of $CaCO_3$.

From Fig. 13 (b), it can be pictured that the thermal decomposition temperature of $CaCO_3$, more obvious for samples cured for 2 h at 5 °C and 20 °C, involved two-stage weight loss, as reported elsewhere [40]. According to Fig. 14, in agreement with [40], two $CaCO_3$ structures were identified: a poorly crystalline $CaCO_3$, decomposed between 500 °C and 650 °C, and a well-defined crystalline $CaCO_3$ structure, decomposed at a temperature above 650 °C [33]. This two-stage decomposition could be resulting from the difference in the thermal stability of the different $CaCO_3$ crystals. As temperature and curing time increase, the well-defined crystalline $CaCO_3$ content increases which is consistent with the Rietveld results presented in Fig. 12. Generally, by comparing the amount of calcite determined by XRD (Fig. 15) to the amount of well-defined crystalline $CaCO_3$ determined by TG-DTG (Fig. 14), it can be seen that the former was higher than the latter. Therefore, it can be speculated that calcite decomposition shifted to a lower temperature (500 °C - 650 °C), or its peak probably overlapped with other phases.

4.4. ^{29}Si NMR characterization

For each temperature, the ^{29}Si NMR spectra of the 28-day CO_2-cured sample were compared to that of the unreacted clinker in Fig. 16. After curing, unreacted C_3S and C_2S (Q^0 located at −71 ppm), observed in the cement clinker, disappeared suggesting that most of C_3S and C_2S have been consumed during the CO_2 curing process. The presence of Q^1 (around −80 ppm) and Q^2 (around −85.5 ppm) provide a clear evidence of the formation of C-S-H gel. This observation confirms the TGA result which revealed a mass loss below 105 °C in particular in the samples cured at 5 °C. Also, the presence of Q^3(Ca) at −99 ppm and Q^4 at −110 ppm indicates the formation of silica gel [41].

To provide a more detailed analysis of the effect of temperature on CO_2-cured pastes, the relative intensities (Q^n%) from the deconvolution

Table 1
Chemical and mineral composition of cement (wt%).

SiO_2	Al_2O_3	Fe_2O_3	CaO	MgO	SO_3	R_2O	f-CaO	C_3S	C_2S	C_3A	C_4AF
21.91	5.30	3.67	64.5	1.51	2.03	0.55	0.88	59.0	16.2	6.8	11.7

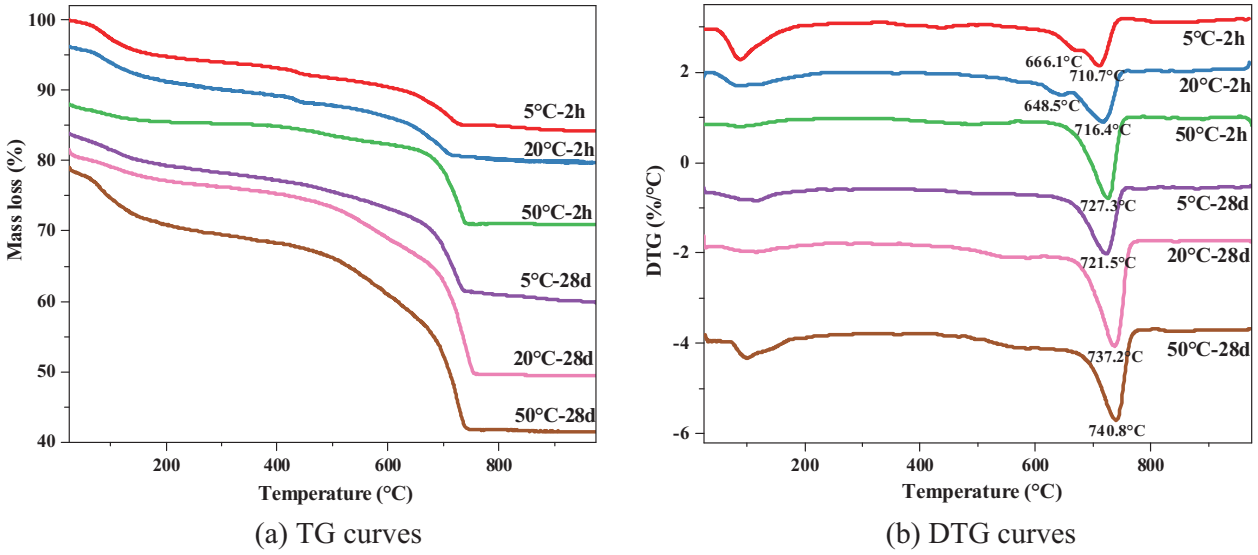

Fig. 13. TG and DTG curves of CO_2-cured pastes at different temperatures.

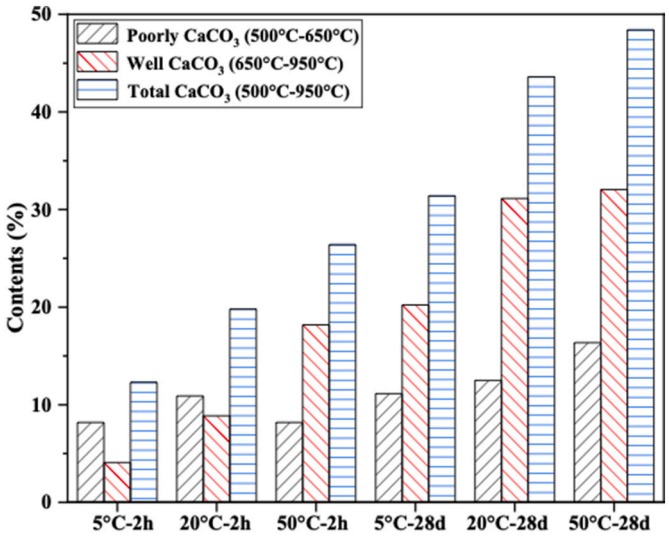

Fig. 14. Poorly and well crystalline $CaCO_3$ contents of CO_2-cured pastes versus temperature.

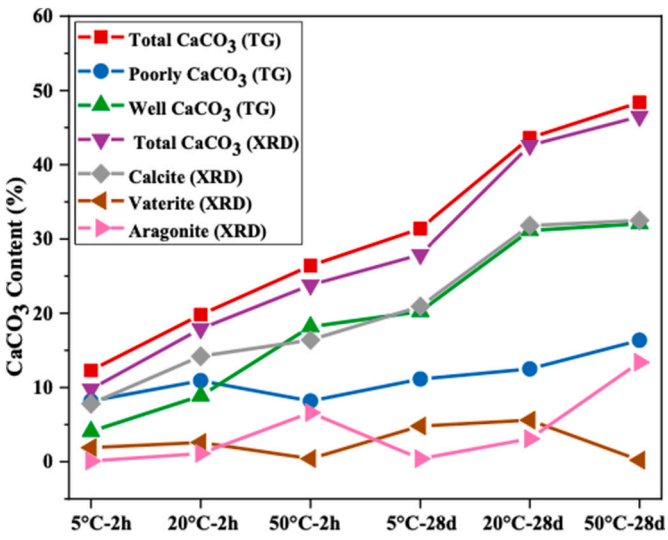

Fig. 15. Comparison of the different $CaCO_3$ crystalline contents determined from DTG and XRD analysis.

results were calculated and summarized in Table 2. At 5 °C, the sample contained only traces of C_3S (Q^0), C_2S (Q^0) and C-S-H gel (Q^1 and Q^2). However, these unreacted phases gradually disappeared in the samples cured at 20 °C and 50 °C. In addition, their Q^2 and Q^4 intensities strongly decreased and increased, respectively, compared to that cured at 5 °C. This result highlights that higher curing temperatures resulted in a higher consumption of clinker phases, namely C_3S and C_2S, and the formation of highly polymerized silica gel. As can be seen in Fig. 16, the silica gel in the samples was completely polymerized and presented a characteristic ^{29}Si NMR silica gel spectra (Q^3 and Q^4). This result demonstrates that the polymerization of silica gel and its Si/Ca ratio could increase with the increase in curing temperature which is in agreement with previous publications [5,42].

4.5. Morphology

Fig. 17 presents the SEM images of CO_2-cured pastes at different temperatures. Despite the similar composition of the samples, the morphology of crystals changed with the increase in temperature. SEM images reveal that (i) calcite (rhombohedral) and vaterite (spheroidal), (ii) calcite, vaterite and aragonite (needle-like shaped crystallites) and (iii) calcite and aragonite (rod-like shaped crystallites) were present in the sample cured at 5 °C, 20 °C and 50 °C, respectively. It is evident that calcite crystals were likely to precipitate at different temperatures due to their high thermodynamic stability with respect to temperature, whereby the metastable phases formed at 5 °C and 50 °C were vaterite and aragonite, respectively. This result is in good agreement with the experimental observations of Deboer [43]. According to Deboer [43], vaterite was stable at low temperatures while the formation of aragonite was dominated by the increase in temperature due to its higher growth rate at high temperatures compared to calcite and vaterite.

On the other hand, temperature had a significant effect on the growth of polymorphs. The size of calcite increased from 250 to 450 nm to 500–2000 nm as temperature increased from 5 °C to 20 °C. At 20 °C, the size of aragonite crystallites was smaller than 1000 nm. At 50 °C, there was a marked change in the morphology of aragonite. At this temperature, most of vaterite traces were gone while the needle-shaped aragonite converted to rod-like aragonite crystallites and their size

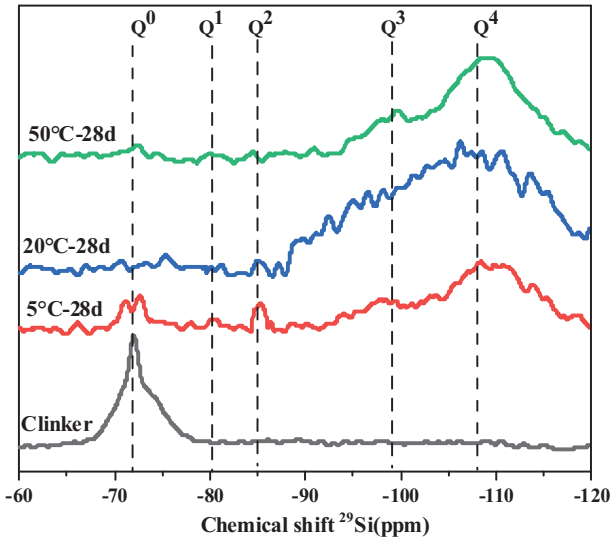

Fig. 16. ^{29}Si NMR spectra of 28 d CO_2-cured pastes at different temperatures.

Table 2
Different Q^n intensities of the CO_2-cured samples at different temperatures.

Samples	Q^n (n = 0–4) intensities/%					
	I(Q^0)	I(Q^1)	I (Q2 p)	I (Q^2)	I(Q^3)	I(Q^4)
5 °C-28 d	8.5	7.6	6.9	12.8	44.4	19.8
20 °C-28 d	2.5	4.3	5.1	9.5	48.5	30.1
50 °C-28 d	1.3	1.9	4.3	6.1	40.2	46.2

became bigger than 3000 nm.

Fig. 18 (a) - (c) presents the BSE images of CO_2-cured pastes at 28 days. The different phases were identified based on the different grey levels in the BSE images [44]. It is obvious that all samples were very dense except for the presence of some minor and small size pores. Fewer pores were observed with increasing temperature suggesting that the increase in the calcite content along with aragonite further contributed to a denser and low porosity matrix than vaterite. It can be seen that the higher was the curing temperature, the lower was the amount of unreacted grains in particular the smallest grains which agrees with XRD results. However, some of the anhydrous cement grains remained unreacted in all samples.

The chemical changes of silica gel in the different paste were examined in terms of element ratios with EDS. The different ratios selected in this study were Al/Ca versus Si/Ca ratio. The circles, shown in Fig. 18 (d), indicate the major atomic ratios that were considered for silica gel with minimal intermixing of secondary phase. Fig. 18 (d) shows that Si/Ca and Al/Ca ratios increased with the increase in temperature, indicating that high temperature resulted in improving the polymerization of silica gel and alumina gel [5,45–48]. A higher Si/Ca ratio could also have contributed to the strength improvement as demonstrated by Kunther et al. [46].

4.6. Nanoindentation analysis

The frequency distribution of the elastic modulus values of the CO_2-cured pastes at different temperatures is exhibited in Fig. 19 and Table 3. Different temperatures resulted basically in the same types of phases namely silica gel, $CaCO_3$ and unreacted cement particles with an average elastic modulus of 35–40 GPa, 64–69 GPa and 117–125 GPa, respectively.

It is clear from Table 3 that the elastic modules of unreacted cement particles decreased with increasing temperature, while the elastic modulus of silica gel increased with increasing temperature. Notably, the increase in temperature to 20 °C and 50 °C reduced the elastic modules of the unreacted cement particles by 1.6% and 6.4% and increased the elastic modulus of silica gel by 11.4% and 14.3%. This result is in agreement with SEM-EDS and BSE-EDS results and accentuates the fact that CO_2 curing and ambient to high temperature consolidate the cement matrix. Furthermore, the calcium carbonate modulus value decreased with the increase in curing temperature. This could probably indicate that vaterite formed at 5 °C had a higher mean elastic modulus than aragonite which was formed at 50 °C as discussed in Section 3.5. This is in agreement with the experimental results in a previous publication [48], which showed that vaterite had the highest mean elastic modulus while aragonite had the lowest mean elastic modulus.

5. Discussions

5.1. Temperature versus time

Similar to conventional curing techniques, high temperature accelerated the carbonation reaction, increased the carbonation rate, improved the strength development rate and influenced the microstructure of cement paste. However, as the curing period was extended, the improvement rate of the overall properties was slowed down regardless of temperature. As discussed previously, high temperature accelerated the formation and growth of $CaCO_3$ at early ages and thereby led to a faster coating of unreacted cement particles and the plugging of the pore structure. Consequently, the ability of CO_2 to further diffuse into the matrix was impeded and thus the effect of temperature on the overall properties was slowed down. The blockage of CO_2 diffusion resulted in a lower carbonation depth increase with time. Referring to Fig. 6, the carbonation depth was notably slowed down with time in particular for the samples cured at 50 °C. The presence of unreacted cement particles spotted in the SEM images seems to correspond well with this observation. Therefore, the decrease in the improvement rate of the overall properties over time could be explained.

5.2. Effect of temperature on the carbonation kinetics

As previous studies illustrated, kinetic parameters depend mostly on experimental conditions, in particular temperature [49]. To evaluate the different reaction kinetics and hence the effect of temperature on the CO_2 curing process, the Arrhenius equation in its logarithmic form (Eq. 1) was used [50]:

$$\ln K = \frac{-Ea}{R} \times \frac{1}{T} + B \quad (1)$$

where K is the reaction rate in mm/s$^{0.5}$, Ea is the activation energy, R (8.314 J/K mol) is the universal gas constant, T is the temperature in Kelvin and B is an intercept.

In this study, the reaction rate was determined as the slope of the fitted line of the carbonation depth-time square root plot and is equal to 2.522 mm/s$^{0.5}$, 3.905 mm/s$^{0.5}$ and 4.997 mm/s$^{0.5}$ at 5 °C, 20 °C and 50 °C, respectively. It is clear that the increase in temperature increased considerably the reaction rate. As known, the increase in the temperature improves the mass transfer rate, promotes the thermal motion of molecules and increases their average kinetic energy which results in speeding up the carbonation reaction [51]. Therefore, it could be speculated that the enhanced reaction rate at elevated temperature had a dominating effect on the carbonation reaction in the first 12 h of the curing process, while the fast precipitation of the carbonate product lowered the carbonation rate later on due to the diffusion limitation of reacting species through the layer [52].

In general, the reaction mechanism governing the carbonation reaction rate is controlled by (1) chemical reaction at the cement particle surface and (2) CO_2 diffusion through the carbonate layers surrounding

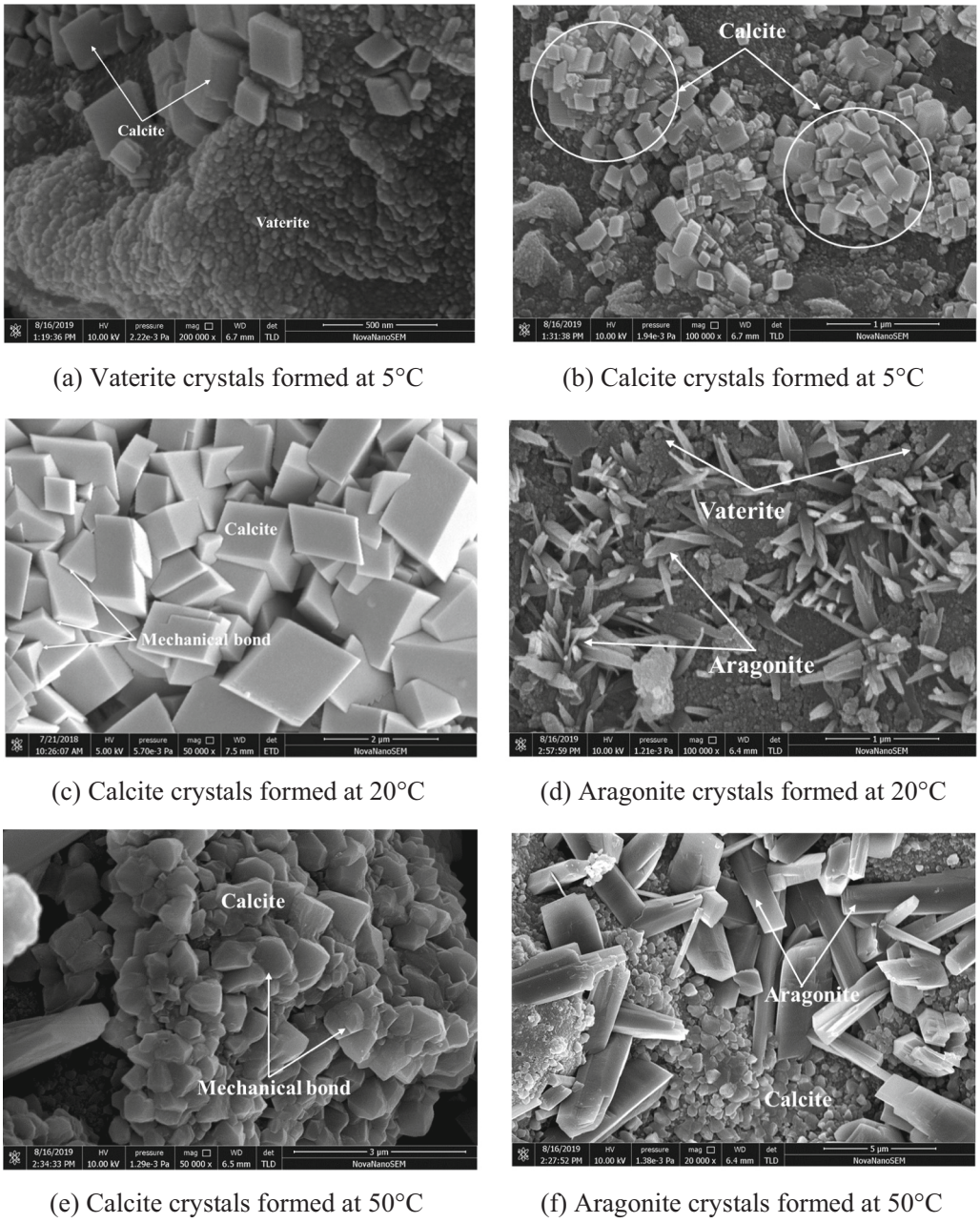

(a) Vaterite crystals formed at 5°C

(b) Calcite crystals formed at 5°C

(c) Calcite crystals formed at 20°C

(d) Aragonite crystals formed at 20°C

(e) Calcite crystals formed at 50°C

(f) Aragonite crystals formed at 50°C

Fig. 17. SEM images of CO_2-cured pastes at different temperatures.

the cement grains. However, the above results showed that temperature increased the reaction rate and consequently influenced the carbonation reaction mechanism. To study further the influence of temperature on the carbonation reaction rate, the activation energy (Ea) was calculated from the slope of the Arrhenius equation, as follows in Fig. 20. In this study, the Ea is about 10.8 kJ/mol, indicating that the product layer diffusion has controlled the CO_2 curing process [53,54]. Again, it could be concluded that initially and for the first 12 h of curing, carbonation was rapid and followed a rate that is chemically rate-controlling mechanism at the surface of cement particles but undergoes a sudden transition to a slower diffusion-controlled regime thereafter. Ashraf et al. [20] reported that the carbonation of calcium silicate phases occurred in two stages, namely phase boundary controlled stage during the initial 10 h of CO_2 exposure and then a product layer diffusion-controlled stage up to the end of the CO_2 exposure. However, higher activation energies (>30 kJ/mol) were reported in their study in particular for the diffusion-controlled stage. This can be due to the differences in the sample mix design as well as the CO_2 curing process.

5.3. *Effect of temperature on the crystallization pathway*

The results of this study showed that the formation of the different polymorphs was controlled by temperature. Nielsen et al. [54] defined two $CaCO_3$ crystallization pathways: direct and indirect. The first one consisted of the direct formation of crystalline polymorphs independently of any amorphous particles. The indirect pathway consisted of the transformation of the amorphous precursor into a more energetically favorable crystalline through a direct, physical connection between the growing and shrinking phases [55]. In this study, low temperature (5 °C) seemed to impair the formation of vaterite and high temperature (50 °C) led to aragonite formation, while calcite was the most prominent crystalline at different temperatures. Based on the work of Nielson et al. [55], the lack of vaterite at high temperature (50 °C) could be attributed to its dissolution. Therefore, it is evident that temperature could be

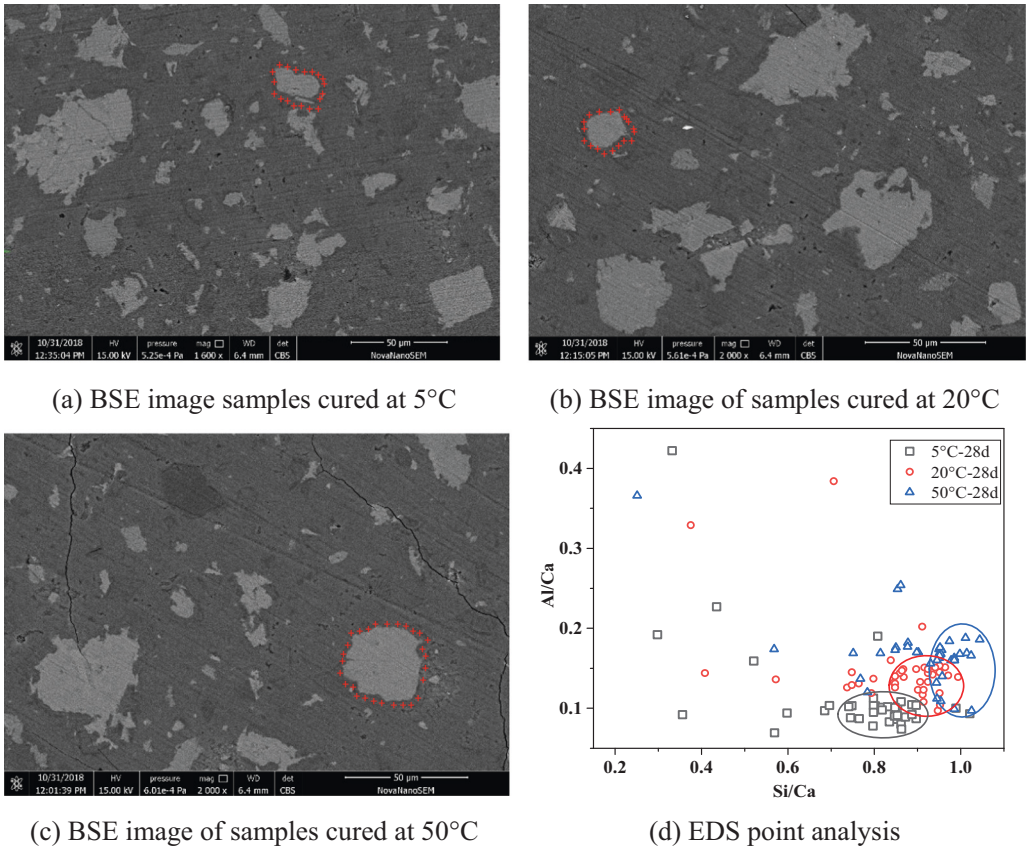

Fig. 18. Typical BSE images and EDS analyses of CO_2-cured samples at different temperatures.

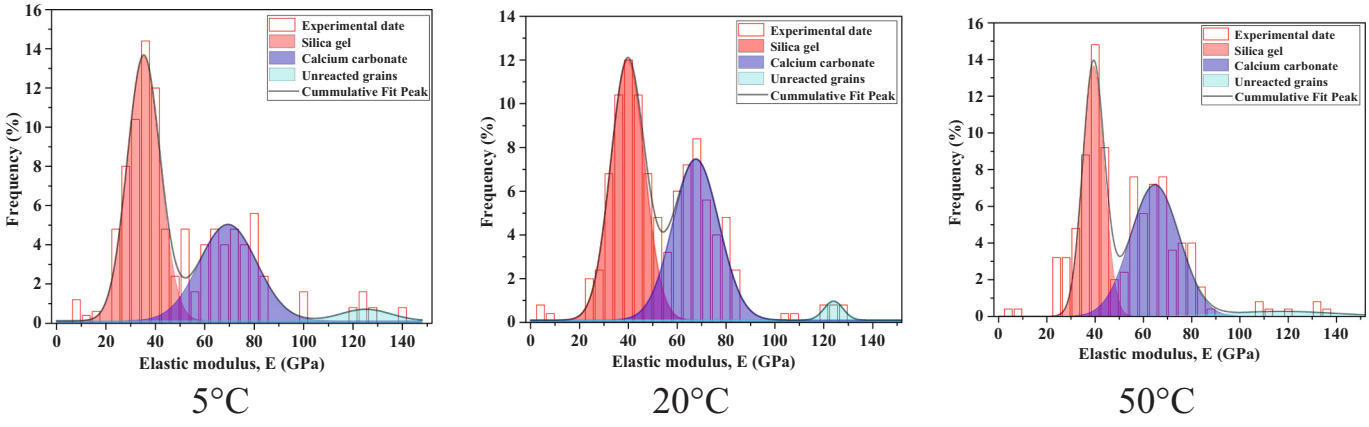

Fig. 19. Frequency distribution and theoretical PDF of elastic modulus of CO_2-cured pastes.

Table 3
The mean elastic modulus of single microscopic phase in CO_2-cured pastes at different temperatures.

Microscopic phase	Mean elastic modulus (GPa)		
	5 °C	20 °C	50 °C
Silica gel	35	39	40
$CaCO_3$	69	67	64
Unreacted clinkers	125	123	117

controlled so as to get either calcite, vaterite, or aragonite or a mixture of calcite, vaterite and aragonite.

5.4. Relation between phase composition and compressive strength

Compressive strength was significantly improved with increasing temperature. The reason for such result could be potentially linked to the effect of temperature on the reaction kinetics and consequently it is effect on the phase composition of the sample as well as the morphological differences of the carbonate polymorphs. According to XRD results, different curing temperatures resulted in different amounts of phases as well as the type and size of polymorphs. There should be also other factors affecting the compressive strength development such as the

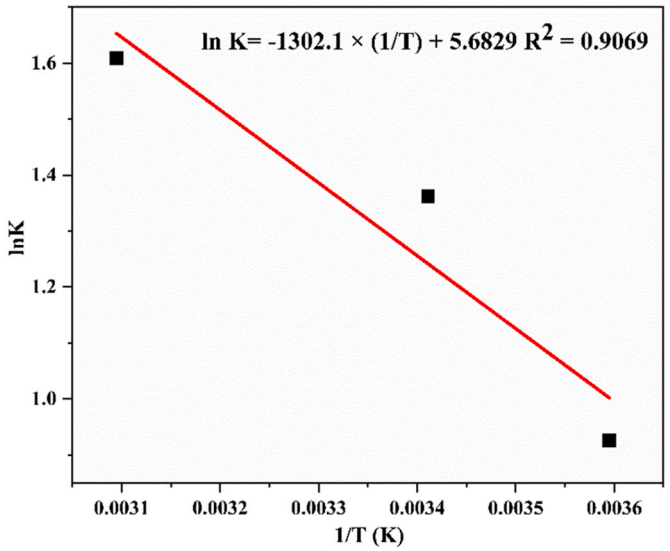

Fig. 20. Regression of Arrhenius equation.

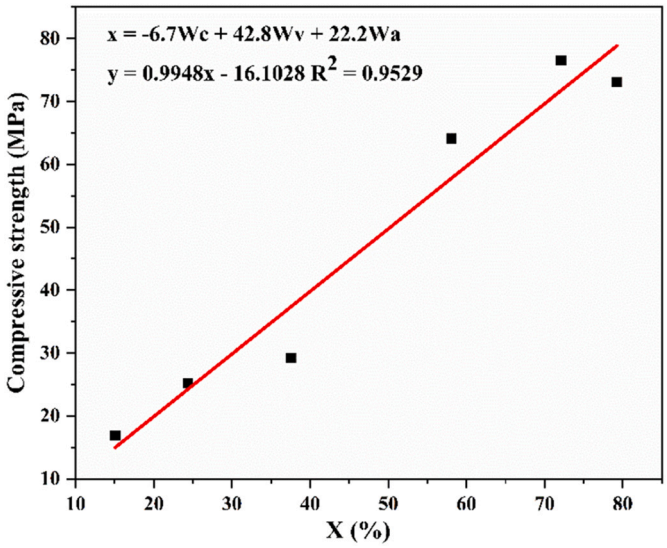

Fig. 21. Relationship between the amount of different crystalline calcium carbonates and compressive strength (Wc, Wa and Wv represent the percentage of calcite, aragonite and vaterite calculated by QXRD, respectively).

porosity, the amount of poorly $CaCO_3$, the increase in crystals size and Si/Ca ratio as observed in the SEM and ^{29}Si NMR spectrums. Note that XRD and TGA results revealed the presence of unreacted cement particles and some hydration products. However, unreacted cement clinker and hydration products have been reported to have a negligible effect on the compressive strength of CO_2-cured samples [1,21].

In the following, a relationship between the amount of different $CaCO_3$ polymorphs (X (%)) and compressive strength is plotted in Fig. 21. It can be seen that aragonite and vaterite had a positive effect on the compressive strength development.

6. Conclusions

This study investigated the compressive strength and morphological changes of cement paste cured using CO_2 and different temperatures. The experimental results showed that the increase in temperature improved significantly the strength of CO_2-cured cement paste. Ambient (20 °C) to high (50 °C) temperature effectively increased the carbonation depth. Typically, samples cured at 20 °C and 50 °C reached a carbonation depth 2 times quicker than those cured at 5 °C. Nevertheless, high temperature (50 °C) and curing time over 12 h inhibited the improvement in carbonation depth. On the other hand, low and high temperature influenced greatly the morphology and growth of $CaCO_3$ polymorphs. Calcite was the most dominant polymorphic form found in all samples, regardless of time and temperature. Vaterite was easily formed at low temperatures, while aragonite was more stable at high temperatures. Generally, bigger calcite and aragonite crystals were formed at high temperatures compared to low temperatures. Besides, the polymerization of silica gel and Si/Ca and Al/Ca ratios increased, at high temperatures. Furthermore, higher temperature increased the elastic modulus of silica gel due to the formation of highly-polymerized silica gel. The CO_2 curing was kinetically regulated by a product layer diffusion while the reaction kinetic in particular at early ages might be also controlled chemically to some extent.

In future studies, the effect of different CO_2 concentrations/pressures along with temperature as well as different supplementary cementitious materials (SCMs) should be further evaluated to provide general insight on the behavior of cement-based materials cured particularly with lower CO_2 concentration.

CRediT authorship contribution statement

Bao Lu: Conceptualization, Methodology, Formal analysis, Investigation, Writing – original draft, Data curation. **Sarra Drissi:** Writing – review & editing. **Jianhui Liu:** Validation. **Xiang Hu:** Validation. **Baixin Song:** Validation. **Caijun Shi:** Resources, Writing – review & editing, Supervision, Project administration, Funding acquisition.

Declaration of competing interest

The authors declared that they have no conflicts of interest to this work.

Acknowledgments

The authors would like to thank the financial support from the National Natural Science Foundation of China (U1605242, 52050410333, 52078204) and the Key Laboratory for Advanced Technology in Environment Protection of Jiangsu Province (JH201802, JH201845) and Science and Technology Program of Jiangsu Province (BZ2020012).

References

[1] C.J. Shi, Y.Z. Wu, Studies on some factors affecting CO2 curing of lightweight concrete products, Resour. Conserv. Recycl. 52 (9) (2008) 1087–1092.
[2] C.J. Shi, D.H. Wang, F.Q. He, et al., Weathering properties of CO2-cured concrete blocks, Resources Conservation Recycling 65 (2012) 11–17.
[3] B.X. Song, C.J. Shi, X. Hu, K. Ouyang, Y.H. Ding, G.J. Ke, et al., Effect of early CO2 curing on the chloride transport and binding behaviors of fly ash- blended Portland cement, Constr. Build. Mater. 288 (2021), 123113.
[4] B. Lu, C.J. Shi, G.H. Hou, et al., Strength and microstructure of CO2 cured low-calcium clinker, Constr. Build. Mater. 188 (2018) 417–423.
[5] T. Chen, X. Gao, Effect of carbonation curing regime on strength and microstructure of Portland cement paste, J. CO2 Utiliz. 34 (2019) 74–86.
[6] X.Y. Pan, C.J. Shi, X. Hu, et al., Effects of CO2 surface treatment on strength and permeability of one-day-aged cement mortar, Constr. Build. Mater. 154 (2017) 1087–1095.
[7] S. Monkman, Y.X. Shao, Integration of carbon sequestration into curing process of precast concrete, Can. J. Civ. Eng. 37 (2) (2008) 302–310.
[8] C.J. Shi, M. Liu, P.P. He, et al., Factors affecting kinetics of CO2 curing of concrete, J. Sustain. Cem. Based Mater. 1 (2) (2012) 24–33.
[9] M. Salman, O. Cizer, Y. Pontikes, et al., Effect of accelerated carbonation on AOD stainless steel slag for its valorisation as a CO2-sequestering construction material, Chem. Eng. J. 246 (2014) 39–52.
[10] Y.X. Shao, M.S. Mirza, X. Wu, CO2 sequestration using calcium-silicate concrete, Can. J. Civ. Eng. 33 (6) (2006) 776–784.
[11] C.J. Shi, F.Q. He, Y.Z. Wu, Effect of pre-conditioning on CO2 curing of lightweight concrete blocks mixtures, Constr. Build. Mater. 26 (1) (2012) 257–267.
[12] E. Drouet, S. Poyet, J. Torrenti, Temperature influence on water transport in hardened cement pastes, Cem. Concr. Res. 76 (2015) 37–50.

[13] T. Ishida, Modeling of carbonation based on thermo-hygro physics with strong coupling of mass transport and equilibrium in micro-pore structure of concrete, J. Adv. Concr. Technol. 6 (2008) 303–316.
[14] J.J. Carroll, J.D. Slupsky, A.E. Mather, The solubility of carbon dioxide in water at low pressure, J. Phys. Chem. 20 (1991) 1201–1209.
[15] L. Liu, J. Ha, T. Hashida, et al., Development of a CO2 solidification method for recycling autoclaved lightweight concrete waste, J. Mater. Sci. Lett. 20 (19) (2001) 1791–1794.
[16] P.S. Humbert, J.P. Castro-Gomes, H. Savastano, Clinker-free CO2 cured steel slag based binder: optimal conditions and potential applications, Constr. Build. Mater. 210 (20) (2019) 413–421.
[17] D. Konopacka-Yskawa, Synthesis methods and favorable conditions for spherical vaterite precipitation: a review, Crystals 9 (4) (2019) 223.
[18] H. Nebel, M. Neumann, C. Mayer, et al., On the structure of amorphous calcium carbonate -a detailed study by solid-state NMR spectroscopy, Inorg. Chem. 47 (17) (2008) 7874–7879.
[19] J. Chen, L. Xiang, Controllable synthesis of calcium carbonate polymorphs at different temperatures, Powder Technol. 189 (1) (2009) 64–69.
[20] W. Ashraf, O. Jan, Carbonation activated binders from pure calcium silicates: reaction kinetics and performance controlling factors, Cem. Concr. Compos. 93 (2018) 85–98.
[21] Z.J. Tu, C.S. Poon, C.J. Shi, et al., Effects of limestone powder on CaCO3 precipitation in CO2 cured cement pastes, Cem. Concr. Compos. 72 (2016) 9–16.
[22] C.J. Goobrake, J.F. Young, Reaction of hydraulic calcium silicates with carbon dioxide and water, J. Am. Ceram. Soc. 62 (9) (1979) 488–491.
[23] T.F. Chen, X.J. Gao, Effect of carbonation curing regime on strength and microstructure of Portland cement paste, J. CO2 Utiliz. 34 (2019) 4–86.
[24] S. Hussain, D. Bhunia, S.B. Singh, Comparative study of accelerated carbonation of plain cement and fly-ash concrete, J. Build. Eng. 10 (2017) 26–31.
[25] A.F. Jamsheer, K. Kupwade-Patil, O. Buyukozturk, et al., Analysis of engineered cement paste using silica nanoparticles and metakaolin using 29Si NMR, water adsorption and synchrotron X-ray diffraction, Constr. Build. Mater. 180 (20) (2018) 698–709.
[26] K. Pasupathy, J. Sanjayan, P. Rajeev, Evaluation of alkalinity changes and carbonation of geopolymer concrete exposed to wetting and drying, J. Build. Eng. 35 (2021), 102029.
[27] C.F. Chang, J.W. Chen, The experimental investigation of concrete carbonation depth, Cem. Concr. Res. 36 (2006) 1760–1767.
[28] S. Monkman, Y.X. Shao, Carbonation curing of slag-cement concrete for binding CO2 and improve performance, J. Mater. Civ. Eng. 22 (4) (2010) 296–304.
[29] B.J. Zhan, D.X. Xuan, C.S. Poon, et al., Mechanism for rapid hardening of cement pastes under coupled CO2-water curing regime, Cem. Concr. Compos. 97 (2019) 78–88.
[30] S. Goto, K. Suenaga, T. Kado, et al., Calcium silicate carbonation products, J. Am. Ceram. Soc. 78 (11) (2010) 2867–2872.
[31] J.D. Rodriguez-Blanco, S. Shaw, L.G. Benning, The kinetics and mechanisms of amorphous calcium carbonate (ACC) crystallization to calcite, via vaterite, Nanoscale 3 (1) (2011) 265–271.
[32] J. Jiang, Q. Zheng, D. Hou, et al., Calcite crystallization in the cement system: morphological diversity, growth mechanism and shape evolution, Phys. Chem. Chem. Phys. 20 (2018) 14174.
[33] H. El-Hassan, Y.X. Shao, Early carbonation curing of concrete masonry units with Portland limestone cement, Cem. Concr. Compos. 62 (2015) 168–177.
[34] J.D. Han, G.H. Pan, W. Sun, et al., Application of nanoindentation to investigate chemomechanical properties change of cement paste in the carbonation reaction, Sci. China Technol. Sci. 55 (3) (2012) 616–622.
[35] J.F. Young, R.L. Berger, J. Breese, Accelerated curing of compacted calcium silicate mortars on exposure to CO2, J. Am. Ceram. Soc. 7 (9) (1974) 394–397, 974.
[36] S. Monkman, P.A. Kenward, G. Dipple, et al., Activation of cement hydration with carbon dioxide, J. Sustain. Cement Based Mater. 7 (3) (2018) 160–181.
[37] X.Y. Pan, C.J. Shi, X. Hu, et al., Effects of CO2 surface treatment on strength and permeability of one-day-aged cement mortar, Constr. Build. Mater. 154 (2017) 1087–1095.
[38] W. Ashraf, J. Olek, Carbonation behavior of hydraulic and non-hydraulic calcium silicates: potential of utilizing low-lime calcium silicates in cement-based materials, J. Mater. Sci. 51 (13) (2016) 6173–6191.
[39] W. Ashraf, J. Olek, S. Sahu, Phase evolution and strength development during carbonation of low-lime calcium silicate cement (CSC), Constr. Build. Mater. 210 (2019) 473–482.
[40] B. Lu, C.J. Shi, J.K. Zhang, et al., Effects of carbonated hardened cement paste powder on hydration and microstructure of Portland cement, Constr. Build. Mater. 186 (2018) 699–708.
[41] M. Auroy, S. Poyet, P. Le Bescop, et al., Comparison between natural and accelerated carbonation (3% CO2): impact on mineralogy, microstructure, water retention and cracking, Cem. Concr. Res. 109 (2018) 64–80.
[42] T.F. Sevelsted, J. Skibsted, Carbonation of C-S-H and C-A-S-H samples studied by 13C, 27Al and 29Si MAS NMR spectroscopy, Cem. Concr. Res. 71 (2015) 56–65.
[43] R.B. Deboer, Influence of seed crystals on the precipitation of calcite and aragonite, Am. J. Sci. 277 (1) (1977) 38–60.
[44] H. Zhang, Y. Xu, Y. Gan, et al., Microstructure informed micromechanical modelling of hydrated cement paste: techniques and challenges, Constr. Build. Mater. 251 (2020), 118983.
[45] X.Y. Pan, C.J. Shi, N. Farzadnia, et al., Properties and microstructure of CO2 surface treated cement mortars with subsequent lime-saturated water curing, Cem. Concr. Compos. 99 (2019) 89–99.
[46] W. Kunther, S. Ferreiro, J. Skibsted, Influence of the Ca/Si ratio on the compressive strength of cementitious calcium-silicate-hydrate binders, J. Mater. Chem. A 5 (2017) 17401–17412.
[47] W. Ashraf, O. Jan, Elucidating the accelerated carbonation products of calcium silicates using multi-technique approach, J. CO2 Utiliz. 23 (2018) 61–74.
[48] R. Ševčík, P. Šašek, A. Viani, Physical and nanomechanical properties of the synthetic anhydrous crystalline CaCO3 polymorphs: vaterite, aragonite and calcite, J. Mater. Sci. 53 (6) (2018) 4022–4033.
[49] G. Grasa, I. Martínez, M.E. Diego, et al., Determination of CaO carbonation kinetics under recarbonation conditions, Energy Fuel 28 (6) (2014) 4033–4042.
[50] E. Drouet, Poyet Stéphane, P. Le Bescop, et al., Carbonation of hardened cement pastes: influence of temperature, Cem. Concr. Res. 115 (2019) 445–459.
[51] L. Ji, H. Yu, R. Zhang, et al., Insights into carbonation kinetics of fly ash from Victorian lignite for CO2 sequestration, Energy Fuel 32 (4) (2018) 4569–4578.
[52] D.K. Lee, An apparent kinetic model for the carbonation of calcium oxide by carbon dioxide, Chem. Eng. J. 100 (1–3) (2004) 71–77.
[53] O. Rahmani, A. Kadkhodaie, J. Highfield, Kinetics analysis of CO2 mineral carbonation using byproduct red gypsum, Energy Fuel 30 (9) (2016) 7460–7464.
[54] M. Gharabaghi, M. Irannajad, A.R. Azadmehr, Leaching kinetics of nickel extraction from hazardous waste by sulphuric acid and optimization dissolution conditions, Chem. Eng. Res. Des. 91 (2) (2013) 325–331.
[55] M.H. Nielsen, S. Aloni, J. De Yoreo, In situ TEM imaging of CaCO3 nucleation reveals coexistence of direct and indirect pathways, Science 345 (6201) (2014) 1158–1162.